*J. Fluid Mech.* (1982), *vol.* 122, *pp.* 273–294
*Printed in Great Britain*



# Axisymmetric stagnation flow of a spherical particle near a finite planar surface at zero Reynolds number

By Z. DAGAN,

Institute of Applied Chemical Physics, The City College of The City University of New York, New York

R. PFEFFER

Department of Chemical Engineering, The City College of The City University of New York, New York

AND S. WEINBAUM

Department of Mechanical Engineering, The City College of The City University of New York, New York

(Received 30 January 1981 and in revised form 18 February 1982)

The general axisymmetric creeping motion of a spherical particle in a stagnation region near a finite surface is modelled by the motion of a sphere of arbitrary size towards a disk for the following conditions: (*a*) pure translation in quiescent fluid, (*b*) uniform flow past a fixed sphere–disk configuration, and (*c*) a neutrally buoyant sphere carried by the fluid towards a disk. The combined analytic and numerical solution procedure is similar to that described in Dagan, Weinbaum & Pfeffer (1982*b*) for the motion of a sphere towards an orifice.

The drag force acting on the sphere and on the disk under the flow conditions mentioned above is presented. In addition, the fluid velocity field has been obtained for the case of uniform flow past a fixed sphere–disk configuration. These solutions show the formation and coalescence of separated regions of closed streamlines adjacent to the sphere and the disk.

## 1. Introduction

In this paper we examine the general axisymmetric creeping motion of a spherical particle in a stagnation region of a finite planar surface. This flow is modelled by studying the axisymmetric motion of a sphere towards a disk of arbitrary size or the uniform flow past such configuration. The solution technique is an application of the combined analytical–numerical procedure described by Dagan, Weinbaum & Pfeffer (1982*b*) for the inverse geometry of a sphere approaching an orifice. The strong-interaction solutions presented herein are also the first to explore the effect of a finite planar boundary on the motion of a sphere.

This stagnation flow has attracted interest in the last few years because of various applications in which a small particle moves in the stagnation region or the wake of a much larger particle. In particular, the determination of the drag force on the small particle is important in problems of agglomeration of aerosols and removal of particulates from flows. A closely related problem was treated by Stimson & Jeffery (1926),

who presented the solution for the drag on two unequal spheres moving with the same velocity. Cooley & O'Neill (1969) gave numerical values for these forces, and Wacholder & Sather (1974) calculated the velocities of pairs of unequal spheres settling under gravity. Recently, Liao & Krueger (1980) presented a collocation solution to a similar system of two spheroids. The advantage of this solution technique is that it can be applied to geometries that do not conform to a natural co-ordinate system, but its convergence is quite slow when the relative volumes of the particles is large. The entire question of the behaviour of a particle in a stagnation region can be generalized by considering uniform flow past a coaxial sphere–disk configuration.

The limiting case of the present flow problem, a disk of infinite radius, was first solved by Brenner (1961), who made use of the spherical bipolar co-ordinate transformation to satisfy the no-slip boundary conditions on the sphere and on the infinite plane wall simultaneously. This geometry, however, cannot admit a stagnation flow which is valid everywhere with uniform velocity at infinity.

The solution technique used in this paper follows closely the procedure described in Dagan *et al.* (1982*b*). Two different stream-function representations are chosen: one for the region to the left of the plane of the disk containing the sphere and one for the remaining infinite half-space to the right of the disk. The no-slip boundary conditions in each region are satisfied on the disk surface in terms of the unknown velocity at the plane of the disk. The two fields are kinematically and dynamically matched by requiring continuity of the velocity and the normal and tangential stress-tensor components at the interface. The dynamic matching condition provides a solution for the interfacial velocity expressed in terms of the remaining unknown constant coefficients in the series solution for the disturbances produced by the sphere. Finally, the no-slip boundary conditions are satisfied at discrete points on the surface of the sphere, yielding numerical results for the spherical coefficients.

Owing to the linearity of the creeping motion equations and the boundary conditions, the general flow problem can be treated as the superposition of two flows: (i) translation of the sphere along a common axis towards a rigidly held disk in a quiescent fluid, (ii) uniform axisymmetric flow past a stationary sphere and disk.

The paper is organized in five sections. Section 2 contains the formulation of the problem. Section 3 presents solutions for both a sphere translating in quiescent fluid and for the uniform flow past a fixed sphere–disk configuration. In § 4 the results for the drag on the disk are presented. Section 5 considers the zero drag motion of a neutrally buoyant sphere carried by the flow towards the disk. Finally, § 6 contains some comments on the extension of the solution technique in future research. This concluding section also gives a discussion of the relative merits of the boundary collocation series technique and two other solution methods, the integral-equation approach and finite-element method, which have been used for solving non-orthogonal or mixed-co-ordinate boundary-value problems in low-Reynolds-number flow.

## 2. Formulation

The problem consists of a sphere of radius $a'$ translating axisymmetrically with a constant velocity $V'$ towards a disk of radius $b'$ held rigidly at a distance $d'$ from the sphere. The fluid at infinity is assumed to have uniform velocity $U'_\infty$. Figure 1 shows the geometry using dimensionless (unprimed) variables and co-ordinates scaled to the

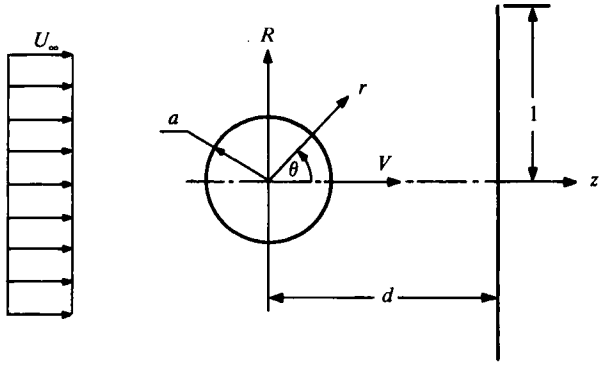


FIGURE 1. Geometry for the problem of a sphere translating axisymmetrically towards a disk.

disk radius. The stream function $\psi'$, the velocity $V'$, the drag force $F'$ and the pressure $p'$ can be expressed in dimensionless form using the fluid density $\rho$, the kinematic viscosity $\nu$ and the disk radius $b'$ as follows:

$$\psi = \frac{\psi'}{b'\nu}, \quad v = \frac{b'}{\nu} V', \quad F = \frac{F'}{\rho\nu^2}, \quad p = \frac{p'b'^2}{\rho\nu^2}. \tag{2.1a–d}$$

The flow field is divided into two regions. The half-space containing the sphere $z < d$, and the infinite half-space $z > d$. Making use of the general solution of the creeping motion equations for axisymmetric flow, one can write the stream function for the region $z \leqslant d$ as the linear superposition

$$\psi^{\mathrm{I}} = \psi_{\mathrm{w}} + \psi_{\mathrm{s}} \tag{2.2}$$

Here $\psi_{\mathrm{w}}$ represents the disturbances produced by the plane of the disk plus a uniform flow at infinity and is given by

$$\psi_{\mathrm{w}} = \tfrac{1}{2}U_\infty R^2 + \int_0^\infty RJ_1(\omega R)\,[A_1(\omega) + zB_1(\omega)]\,e^{\omega z}\,d\omega, \tag{2.3}$$

where $A_1(\omega)$ and $B_1(\omega)$ are unknown functions of $\omega$, and $J_1$ is the ordinary Bessel function of the first kind of order one.

The second part in (2.2), $\psi_{\mathrm{s}}$, represents the disturbances generated by the sphere, written in spherical co-ordinates, and is given by

$$\psi_{\mathrm{s}} = \sum_{n=2}^{\infty} (B_n r^{-n+1} + D_n r^{-n+3})\, I_n(\xi). \tag{2.4}$$

Here $\xi = \cos\theta$, $B_n$ and $D_n$ are unknown constant coefficients, and $I_n$ is the Gegenbauer function of order $n$ and degree $-\frac{1}{2}$.

For the region $z \geqslant d$, a Fourier–Bessel integral representation is chosen for the stream function in the form of (2.3) which yields a uniform velocity as $z$ approaches infinity,

$$\psi^{\mathrm{II}} = \tfrac{1}{2}U_\infty R^2 + \int_0^\infty RJ_1(\omega R)\,[A_2(\omega) + zB_2(\omega)]\,e^{-\omega z}\,d\omega, \tag{2.5}$$

where $A_2(\omega)$ and $B_2(\omega)$ are unknown functions of $\omega$.

The velocity components at the plane of the disk can be defined in a general form by:

$$\mathbf{U}(R,d) = (1/R)\{[f(R)+RU_\infty]\hat{\mathbf{z}} - g(R)\hat{\mathbf{r}}\} \quad (1 < R < \infty). \tag{2.6}$$

The kinematic boundary conditions in the matching plane $z = d$ require that the velocity vanish for $R \leqslant 1$ and that the velocity be continuous for $R \geqslant 1$.

$$\left.\begin{aligned} u_z^i(R,d) &= f(R)/R + U_\infty \quad (1 < R) \\ &= 0 \qquad\qquad\quad (0 \leqslant R \leqslant 1) \end{aligned}\right\} \quad (i = \mathrm{I}, \mathrm{II}), \tag{2.7a}$$

$$\left.\begin{aligned} u_R^i(R,d) &= -g(R)/R \quad (1 < R) \\ &= 0 \qquad\qquad (0 \leqslant R \leqslant 1) \end{aligned}\right\} \quad (i = \mathrm{I}, \mathrm{II}). \tag{2.7b}$$

In addition, the dynamic matching of the two fields requires that the normal and tangential components of the stress tensor be continuous at the interface between the two regions. This condition can be replaced as shown in Dagan *et al.* (1982*a*) by matching the pressure and its gradient. Namely,

$$p^{\mathrm{I}}(R,d) = p^{\mathrm{II}}(R,d), \tag{2.8a}$$

$$\frac{\partial p^{\mathrm{I}}}{\partial z}(R,d) = \frac{\partial p^{\mathrm{II}}}{\partial z}(R,d). \tag{2.8b}$$

Application of the kinematic boundary conditions (2.7*a*, *b*) leads to solutions for $A_1(\omega)$ and $B_1(\omega)$ in terms of the unknown constant coefficients in the spherical solution $\psi_s$ and the unknown velocity functions $f(R)$ and $g(R)$. The resulting velocity field in region I is given by

$$u_R^{\mathrm{I}} = \int_0^\infty \left\{(\omega x - 1)\int_1^\infty g(t)\,J_1(\omega t)\,dt + U_\infty x J_1(\omega) - \omega x \int_1^\infty f(t)\,J_0(\omega t)\,dt\right\} \omega J_1(\omega R)\,e^{-\omega x}\,d\omega + \sum_{n=2}^{\infty}[B_n\beta_n'(R,z) + D_n\delta_n'(R,z)], \tag{2.9a}$$

$$u_z^{\mathrm{I}} = U_\infty + \int_0^\infty \left\{(1+\omega x)\int_1^\infty f(t)\,J_0(\omega t) - \left(\frac{1}{\omega}+x\right)U_\infty J_1(\omega) - \omega x\int_1^\infty g(t)\,J_1(\omega t)\,dt\right\} \omega J_0(\omega R)\,e^{-\omega x}\,d\omega + \sum_{n=2}^{\infty}[B_n\beta_n''(R,z) + D_n\delta_n''(R,z)], \tag{2.9b}$$

where $x = d - z$ and $\beta_n'$, $\delta_n'$, $\beta_n''$, $\delta_n''$ are given in appendix A.

Similarly, an expression for the velocity field $\mathbf{u}^{\mathrm{II}}$ can be obtained:

$$u_R^{\mathrm{II}} = -\int_0^\infty \left\{(1+\omega x)\int_1^\infty g(t)\,J_1(\omega t)\,dt - xU_\infty J_1(\omega) + \omega x\int_1^\infty f(t)\,J_0(\omega t)\,dt\right\} \omega J_1(\omega R)\,e^{\omega x}\,d\omega, \tag{2.10a}$$

$$u_z^{\mathrm{II}} = U_\infty + \int_0^\infty \left\{(1-\omega x)\int_1^\infty f(t)\,J_0(\omega t)\,dt - (1-\omega x)\,U_\infty\frac{J_1(\omega)}{\omega} - \omega x\int_1^\infty g(t)\,J_1(\omega t)\,dt\right\} \omega J_0(\omega R)\,e^{\omega x}\,d\omega. \tag{2.10b}$$

In order to apply the pressure-matching conditions (2.8), the expression for the pressure field in each region is obtained by integrating the creeping-motion equations

with the appropriate stream-function representation. For the half-space containing the sphere the result is

$$p^{\mathrm{I}}(R,z) = 2\int_0^\infty \omega J_0(\omega R)\, B_1(\omega)\, e^{\omega z}\, d\omega + 2\sum_{n=2}^{\infty} D_n \frac{2n-3}{n}\frac{P_n(\xi)}{r^n} \tag{2.11a}$$

and for the infinite half-space $z > d$

$$p^{\mathrm{II}}(R,z) = 2\int_0^\infty \omega J_0(\omega R)\, B_2(\omega)\, e^{-\omega z}\, d\omega \tag{2.11b}$$

where the expressions for $B_i(\omega)$, $i = 1, 2$, are given in appendix B. Application of the pressure-matching conditions results in

$$\int_0^\infty \omega f^*(\omega)\, J_0(\omega R)\, d\omega = F^*(R) \quad (1 < R < \infty), \tag{2.12a}$$

$$\int_0^\infty \omega g^*(\omega)\, J_0(\omega R)\, d\omega = G^*(R) \quad (1 < R < \infty), \tag{2.12b}$$

where

$$f^*(\omega) = \omega\int_0^\infty f(t)\, J_0(\omega t)\, dt - U_\infty J_1(\omega), \tag{2.13a}$$

$$g^*(\omega) = \omega^2\int_1^\infty g(t)\, J_1(\omega t)\, dt, \tag{2.13b}$$

and $F^*$ and $G^*$ are given in appendix C.

The integral equations (2.12) together with

$$\int_0^\infty f^*(\omega)\, J_0(\omega R)\, d\omega = -U_\infty \quad (0 \leqslant R \leqslant 1), \tag{2.14a}$$

$$\int_0^\infty g^*(\omega)\, J_0(\omega R)\, d\omega = 0 \quad (0 \leqslant R \leqslant 1) \tag{2.14b}$$

comprise two sets of dual integral equations for $f^*$ and $g^*$. The solution of (2.12) and (2.14) follows from the results of Tranter (1951), yielding

$$\begin{Bmatrix} f^*(\omega) \\ g^*(\omega) \end{Bmatrix} = \begin{Bmatrix} M_f(\omega) \\ M_g(\omega) \end{Bmatrix} - \frac{2}{\pi}\int_0^1 dt \cos t\omega \int_0^\infty ds \cos ts \begin{Bmatrix} M_f(s) \\ M_g(s) \end{Bmatrix} - \begin{Bmatrix} \frac{2}{\pi} U_\infty \dfrac{\sin\omega}{\omega} \\ 0 \end{Bmatrix}, \tag{2.15}$$

where

$$\begin{Bmatrix} M_f(\omega) \\ M_g(\omega) \end{Bmatrix} = \int_0^\infty \xi \begin{Bmatrix} F^*(\xi) \\ G^*(\xi) \end{Bmatrix} J_0(\omega\xi)\, d\xi. \tag{2.16}$$

The functions $F^*$ and $G^*$ are now substituted into (2.16) and integrated. Then $M_f$ $M_g$ are substituted into (2.15), where the inner integral can be performed analytically. The solutions for $f^*$ and $g^*$ are substituted back into the velocity-field expressions. After considerable algebraic manipulation one obtains

$$u_R^{\mathrm{I}} = \sum_{n=2}^{\infty}\left\{B_n\left[B_n'(R,z) - \frac{2}{\pi}\int_0^1 \mathscr{B}_n^*(R,z,t)\, dt\right] + D_n\left[D_n'(R,z) - \frac{2}{\pi}\int_0^1 \mathscr{D}_n^*(R,z,t)\, dt\right]\right\} + \frac{2}{\pi} U_\infty x S_1^0(R,x), \tag{2.17a}$$

$$u_z^{\mathrm{I}} = \sum_{n=2}^{\infty}\left\{B_n\left[B_n''(R,z) - \frac{2}{\pi}\int_0^1 \mathscr{B}_n^{**}(R,z,t)\, dt\right] + D_n\left[D_n''(R,z) - \frac{2}{\pi}\int_0^1 \mathscr{D}_n^{**}(R,z,t)\, dt\right]\right\} + U_\infty\left\{1 - \frac{2}{\pi}[S_0^{-1}(R,x) + xS_0^0(R,x)]\right\}, \tag{2.17b}$$

where the functions $\mathscr{B}_n^*$, $\mathscr{B}_n^{**}$, $\mathscr{D}_n^*$, $\mathscr{D}_n^{**}$ and $S_\nu^\mu$ are defined in appendix D.

The only boundary conditions that remain to be satisfied are those on the sphere surface

$$u_R = 0, \quad u_z = V, \tag{2.18a, b}$$

where $V$ is the velocity with which the sphere is translating towards the disk. The collocation technique presented in Dagan *et al.* (1982*b*) may now be used for this purpose. At $r = a$, boundary conditions (2.18) are applied at $M$ discrete points and the series solution (2.17) is truncated after $M$ terms. This generates a system of $2M$ linear algebraic equations for $2M$ unknown coefficients $B_n$ and $D_n$ of the spherical solution. The solution for the velocity field is completely known once these coefficients are determined.

The hydrodynamic force acting on the sphere is found from Happel & Brenner (1973, p. 115) to be

$$F = 4\pi D_2. \tag{2.19}$$

Using the hydrodynamic interaction coefficient $\lambda$, one can write the drag force on a sphere translating coaxially with velocity $V$ towards the disk in quiescent fluid as

$$F = 6\pi a V \lambda^{(V)}. \tag{2.20a}$$

For the case of uniform flow past a rigidly held sphere situated axisymmetrically at a distance $d$ from a disk, the drag force is given by

$$F = 6\pi a U_\infty \lambda^{(U_\infty)}. \tag{2.20b}$$

Equating expressions (2.19) and (2.20), one finds

$$\lambda^{(V)} = \frac{D_2^{(V)}}{1{\cdot}5aV}, \tag{2.21a}$$

$$\lambda^{(U_\infty)} = \frac{D_2^{(U_\infty)}}{1{\cdot}5aU_\infty}. \tag{2.21b}$$

In the general case, when both the fluid and the sphere are in motion, the drag force is given by

$$F = 6\pi a(V\lambda^{(V)} + U_\infty \lambda^{(U_\infty)}). \tag{2.22}$$

## 3. Solutions for the motion of a sphere towards a disk

In this section, collocation solutions for the general axisymmetric motion of the sphere will be presented for both (*a*) translation of the sphere in quiescent fluid and (*b*) uniform flow past the fixed sphere–disk configuration.

Before proceeding with the presentation of these results it should be noted that (2.17) can be simplified for the limiting case, a disk of infinite radius, by substituting the dimensional variables and allowing $b'$ to approach infinity. The resulting equations for the velocity field are

$$u_R^{\mathrm{I}} = \sum_{n=2}^{\infty} [B_n \beta_n'(R,z) + D_n \delta_n''(R,z)], \tag{3.1a}$$

$$u_z^{\mathrm{I}} = \sum_{n=2}^{\infty} [B_n \beta_n''(R,z) + D_n \delta_n''(R,z)]. \tag{3.1b}$$

Equations (3.1*a*, *b*) represent the solution for the problem of a sphere translating perpendicular to an infinite plane wall. Application of the collocation technique for

(*a*)

| $d/a$ | $M$ | $a = 0{\cdot}1$ | $a = 0{\cdot}5$ | $a = 1{\cdot}0$ | $a = 10$ |
|---|---|---|---|---|---|
| 5·0 | 6 | −1·2877 | −1·2154 | −1·1166 | −1·0112 |
| | 8 | −1·2877 | −1·2154 | −1·1166 | −1·0112 |
| 2·0 | 6 | −2·1258 | −2·1798 | −1·8930 | −1·0619 |
| | 8 | −2·1258 | −2·1798 | −1·8936 | −1·0619 |
| | 10 | −2·1258 | −2·1798 | −1·8936 | −1·0620 |
| | 12 | — | — | −1·8936 | −1·0620 |
| | 14 | — | — | −1·8936 | −1·0620 |
| 1·5 | 8 | −3·2054 | −3·2951 | −3·0812 | −1·1059 |
| | 10 | −3·2055 | −3·2952 | −3·0813 | −1·1048 |
| | 12 | −3·2055 | −3·2952 | −3·0812 | −1·1046 |
| | 14 | −3·2055 | −3·2952 | −3·0812 | −1·1046 |
| 1·1 | 16 | −11·458 | −11·559 | −11·786 | −1·6444 |
| | 18 | −11·459 | −11·559 | −11·784 | −1·5708 |
| | 20 | −11·459 | −11·559 | −11·784 | −1·5338 |
| | 22 | −11·459 | −11·559 | −11·784 | −1·5238 |
| | 24 | — | — | — | −1·5299 |
| | 26 | — | — | — | −1·5417 |
| | 28 | — | — | — | −1·5519 |
| | 30 | — | — | — | −1·5579 |
| | 32 | — | — | — | −1·5600 |
| | 34 | — | — | — | −1·5601 |
| | 36 | — | — | — | −1·5595 |

(*b*)

| $d/a$ | $M$ | $a = 0{\cdot}1$ | $a = 0{\cdot}5$ | $a = 1{\cdot}0$ | $a = 10$ |
|---|---|---|---|---|---|
| 5·0 | 6 | 0·052987 | 0·65463 | 0·84075 | 0·98575 |
| | 8 | 0·052987 | 0·65463 | 0·84075 | 0·98575 |
| 2·0 | 6 | 0·0065800 | 0·37085 | 0·77523 | 0·99701 |
| | 8 | 0·0065800 | 0·37097 | 0·77459 | 0·99700 |
| | 10 | 0·0065800 | 0·37097 | 0·77463 | 0·99699 |
| | 12 | — | 0·37097 | 0·77463 | 0·99699 |
| | 14 | — | — | 0·77463 | 0·99699 |
| 1·5 | 8 | 0·0035577 | 0·27703 | 0·75386 | 1·0075 |
| | 10 | 0·0035578 | 0·27702 | 0·75383 | 1·0076 |
| | 12 | 0·0035578 | 0·27702 | 0·75391 | 1·0076 |
| | 14 | 0·0035578 | 0·27702 | 0·75390 | 1·0076 |
| | 16 | — | — | 0·75390 | — |
| 1·1 | 16 | 0·0019244 | 0·19204 | 0·73206 | 1·0083 |
| | 18 | 0·0019244 | 0·19204 | 0·73200 | 1·0085 |
| | 20 | 0·0019244 | 0·19204 | 0·73200 | 1·0086 |
| | 22 | — | — | 0·73200 | 1·0086 |
| | 24 | — | — | — | 1·0086 |
| | 26 | — | — | — | 1·0085 |
| | 28 | — | — | — | 1·0084 |

TABLE 1. Convergence of (*a*) $\lambda^{(\Psi)}$ and (*b*) $\lambda^{(U_\infty)}$ for various sphere radii and sphere-to-disk spacings

this case was demonstrated in Dagan *et al.* (1982*b*) and compared with the exact solution of Brenner (1961). Convergence to five significant figures was achieved by the collocation solution for all spacings tested in the range $1{\cdot}1 \leqslant d/a \leqslant 10{\cdot}1$.

As in the case of the motion of a sphere towards an orifice, the most advantageous collocation boundary point to choose is $\theta = \frac{1}{2}\pi$, since this point has the greatest control of the projected area of the sphere normal to its direction of motion. In addition, the points $\theta = 0, \pi$ are important because they control the gap between the sphere and the disk and are known to have increasing effect on the speed of convergence of the results as the gap between the sphere and the disk is made very small. Unfortunately, the coefficient matrix becomes singular if these points are used. Therefore, convergence trials for the force coefficient using four adjacent points $\theta = 0+\delta, \frac{1}{2}\pi \pm \delta, \pi - \delta$ as $\delta \to 0$ were conducted. Tables presenting the results of these tests are contained in Dagan (1980) and have been omitted for brevity. Convergence for $\lambda^{(F)}$ and $\lambda^{(U_\infty)}$ is obtained to five significant figures for $\delta \leqslant 0{\cdot}01$ at all spacings tested.

The rate of convergence of the solutions as the number of boundary points is increased is examined for various spacings and sphere radii in tables 1 (*a* and *b*). The starting value of $M$ for a given case in these tables is based on the results of similar tests conducted for the motion of a sphere towards an orifice. The slowest rate of convergence is found at $d/a = 1{\cdot}1$ and $a = 10$ for the two flows considered. Convergence to only three significant figures is obtained with $M = 34$ for the sphere translating towards the disk and $M = 22$ for the flow past a stationary sphere-and-disk configuration. Therefore for large values of $a$ and small spacings, where convergence is slow, the solutions presented are accurate only to three significant digits. The slow rate of convergence for the case of the sphere translating towards the disk can be explained by the fact that large fluid velocities can be generated in the intervening fluid gap when its dimensions become small compared with the sphere radius. In the case of flow past a stationary sphere–disk configuration the slow convergence is due to the complexity of the flow in the gap between the two surfaces.

The final results for the hydrodynamic interaction coefficients $\lambda^{(F)}$ and $\lambda^{(U_\infty)}$ are shown in figures 2 and 3. In addition, for reference, converged values are presented in tables 2 and 3. Examination of the results reveals two interesting features. First, in the case of a sphere translating towards a disk (table 2) the force acting on a sphere smaller than the disk increases above the value of the force acting on a sphere translating perpendicular towards an infinite plane wall ($a = 0$), and approaches that value as the sphere approaches the disk. These results can be explained by the fact that the edge of a finite disk introduces a strong resistance to the fluid motion demonstrated by the singularity in the pressure field at $R = 1$. This resistance can be greater than the total integrated resistance along an infinite wall where the fluid motion is almost parallel to the boundary. Hence a larger force is required to push the fluid around the hinge point $R = 1$ than along an infinite boundary. When the spacing between the sphere and the disk decreases further, the edge effect is diminished, and the flow field in the vicinity of the sphere resembles the flow for the case of a sphere approaching an infinite wall.

The second interesting result is observed for the case of uniform flow past a rigidly held sphere-and-disk configuration. Here, for spheres larger than the disk, the drag force acting on the sphere for values of $d/a$ near $1{\cdot}0$ becomes slightly larger than the force acting on an isolated sphere in a uniform stream. These results motivated

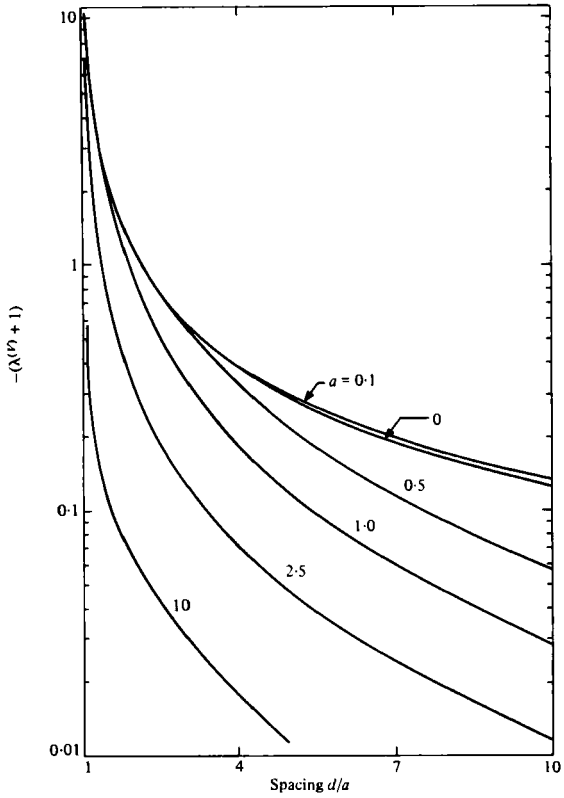


FIGURE 2. Drag on a sphere translating axisymmetrically towards a disk.

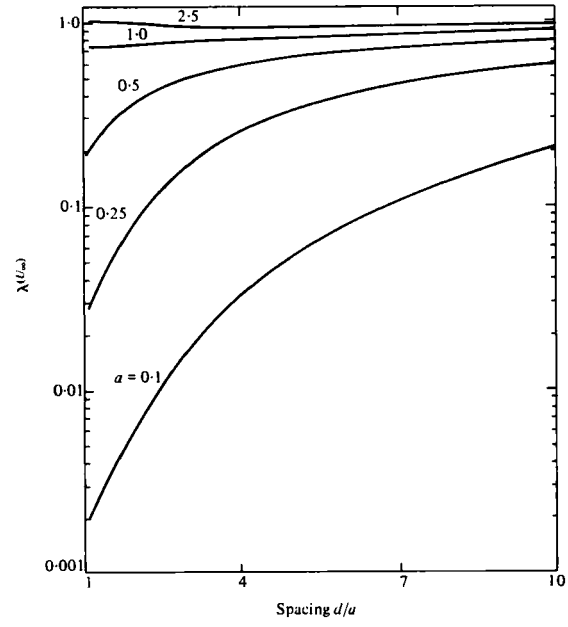


FIGURE 3. Drag on a rigidly held sphere in a uniform flow past a sphere–disk configuration.

| $\frac{d}{a}$ \ $a$ | 0† | 0·1 | 0·25 | 0·5 | 0·75 | 1·0 | 2·5 | 5·0 | 7·5 | 10 |
|---|---|---|---|---|---|---|---|---|---|---|
| 1·1 | −11·459 | −11·459 | −11·464 | −11·559 | −11·768 | −11·784 | −7·09 | −3·04 | −1·96 | −1·56 |
| 1·25 | −5·3053 | −5·3054 | −5·3123 | −5·4051 | −5·5172 | −5·3773 | −2·8182 | −1·5704 | −1·2854 | −1·1790 |
| 1·5 | −3·2054 | −3·2055 | −3·2147 | −3·2952 | −3·2954 | −3·0812 | −1·7048 | −1·2643 | −1·1513 | −1·1046 |
| 2·0 | −2·1255 | −2·1258 | −2·1394 | −2·1798 | −2·0776 | −1·8936 | −1·3152 | −1·1354 | −1·0851 | −1·0620 |
| 3·0 | −1·5692 | −1·5700 | −1·5878 | −1·5543 | −1·4392 | −1·3417 | −1·1292 | −1·0613 | −1·0401 | −1·0297 |
| 4·0 | −1·3802 | −1·3818 | −1·3953 | −1·3272 | −1·2417 | −1·1848 | −1·0719 | −1·0350 | −1·0231 | −1·0172 |
| 5·0 | −1·2851 | −1·2877 | −1·2916 | −1·2154 | −1·1536 | −1·1166 | −1·0459 | −1·0226 | −1·0150 | −1·0112 |
| 6·0 | −1·2279 | −1·2314 | −1·2247 | −1·1521 | −1·1064 | −1·0805 | −1·0318 | −1·0158 | −1·0105 | −1·0078 |
| 8·0 | −1·1625 | −1·1672 | −1·1440 | −1·0872 | −1·0579 | −1·0450 | −1·0179 | −1·0089 | −1·0059 | −1·0044 |
| 10·0 | −1·1262 | −1·1305 | −1·0989 | −1·0563 | −1·0382 | −1·0287 | −1·0115 | −1·0057 | −1·0038 | −1·0028 |

† Solution for a sphere translating perpendicular to an infinite plane wall, $b' \to \infty$ (Brenner 1961).

TABLE 2. Drag correction factor $\lambda^{(V)}$ for a sphere translating axisymmetrically towards a disk for various sphere radii $a$ and sphere-to-disk spacings $d/a$

| $\frac{d}{a}$ \ $a$ | 0·1 | 0·25 | 0·5 | 0·75 | 1·0 | 2·5 | 5·0 | 7·5 | 10·0 |
|---|---|---|---|---|---|---|---|---|---|
| 1·1 | 0·0019244 | 0·028422 | 0·19204 | 0·47616 | 0·73200 | 1·03 | 1·02 | 1·01 | 1·0 |
| 1·25 | 0·0024625 | 0·035592 | 0·24449 | 0·51115 | 0·74093 | 1·01 | 1·02 | 1·01 | 1·01 |
| 1·5 | 0·0035578 | 0·049394 | 0·27702 | 0·55879 | 0·75390 | 0·99551 | 1·0104 | 1·0092 | 1·0076 |
| 2·0 | 0·0065800 | 0·083163 | 0·37097 | 0·62668 | 0·77463 | 0·96585 | 0·99090 | 0·99536 | 0·99699 |
| 3·0 | 0·016469 | 0·16675 | 0·50853 | 0·70483 | 0·80212 | 0·94086 | 0·97337 | 0·98282 | 0·98732 |
| 4·0 | 0·031980 | 0·25566 | 0·59599 | 0·74920 | 0·82271 | 0·93780 | 0·97027 | 0·98047 | 0·98545 |
| 5·0 | 0·052987 | 0·33751 | 0·65463 | 0·78023 | 0·84075 | 0·94080 | 0·97114 | 0·98093 | 0·98575 |
| 6·0 | 0·078730 | 0·40790 | 0·69705 | 0·80424 | 0·85637 | 0·94516 | 0·97303 | 0·98212 | 0·98663 |
| 8·0 | 0·13985 | 0·51603 | 0·75559 | 0·83961 | 0·88101 | 0·95351 | 0·97696 | 0·98468 | 0·98853 |
| 10·0 | 0·20622 | 0·59223 | 0·79480 | 0·86444 | 0·89898 | 0·95016 | 0·98019 | 0·98682 | 0·99012 |

TABLE 3. Drag correction factor $\lambda^{(U_\infty)}$ for a flow past a stationary sphere situated coaxially near a disk for various sphere radii $a$ and sphere-to-disk spacings $d/a$

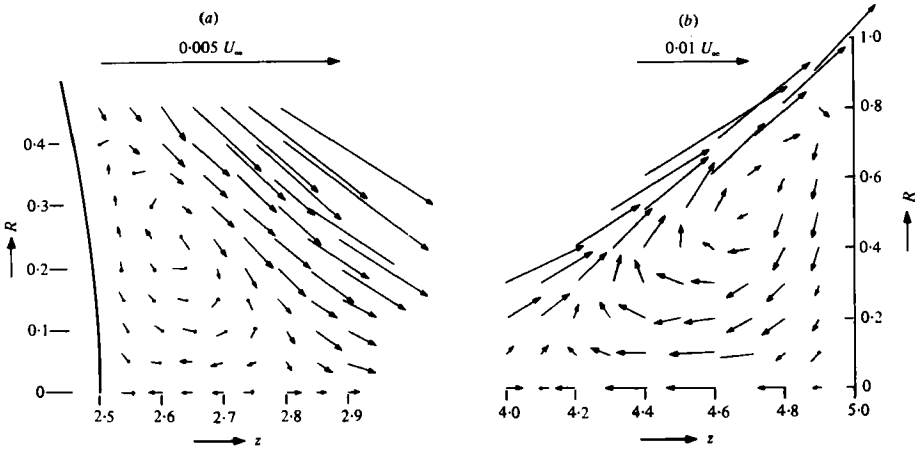


FIGURE 4. Separated ring vortices near (*a*) sphere surface and (*b*) the disk; $a = 2{\cdot}5$, $d/a = 2$.

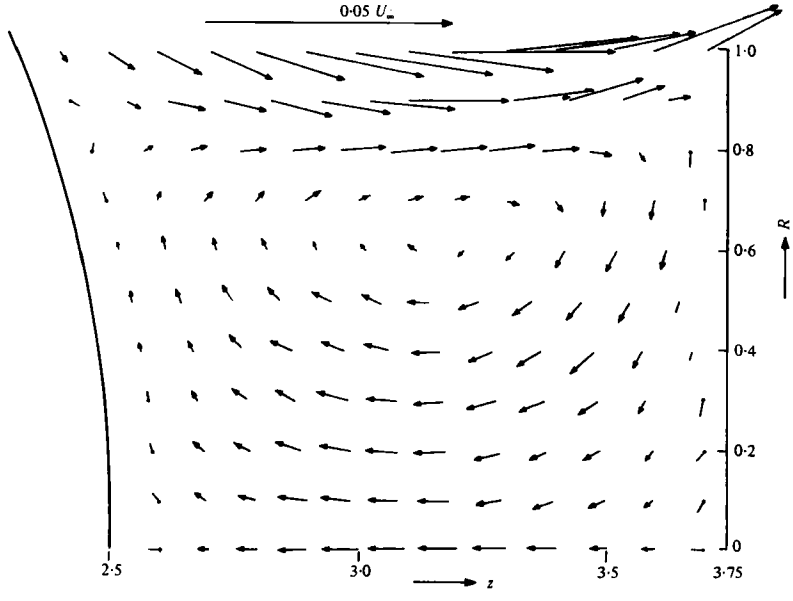


FIGURE 5. The flow structure after coalescence of the two primary ring vortices; $a = 2{\cdot}5$; $d/a = 1{\cdot}5$.

additional tests to assure that convergence was actually achieved. In the cases in question the number of boundary points was increased much beyond the upper limit shown in table 3. Owing to the limitation of excessive computation time when the spacing is small the tests were conducted for intermediate spacings up to $d/a = 1{\cdot}5$ (e.g., for $a = 10$ and $d/a = 0{\cdot}5$, 28 points were selected). The results obtained from these tests matched the values in table 3 exactly.

To help understand this intriguing behaviour the velocity field was examined for $a = 2{\cdot}5$ and various spacings. Figures 4 and 5 show the velocity field for the flow past

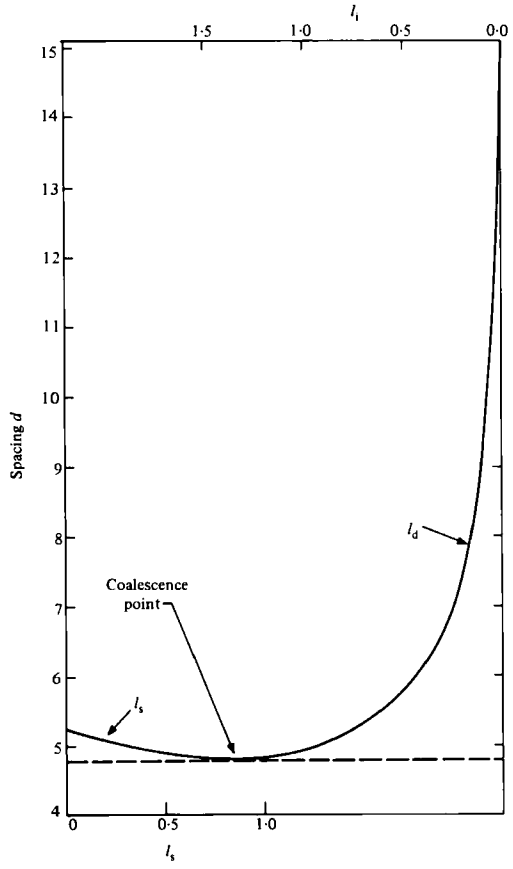


FIGURE 6. Wake size: $l_s$ for the sphere wake; $l_d$ for the disk wake. $a = 2{\cdot}5$.

a sphere–disk configuration in the gap between the two objects. The velocity vectors shown with arrowheads have been drawn to scale, and show the magnitude and direction of the fluid motion. For cases where the magnitude of the velocity is too small to be visible on the scale shown the direction of the fluid motion is shown by a straight line without an arrow at the indicated point. Figure 4 shows the flow field at $d/a = 2$. Two separated regions of trapped fluid are visible on the sides of the sphere and the disk facing each other (additional computations have shown that there are no separated regions in front of the sphere and behind the disk). The flow field shown is similar to the one presented in Davis *et al.* (1976) for the flow past two equal spheres. At closer spacing ($d/a = 1{\cdot}5$, figure 5) the wakes coalesce, and the two ring vortices have merged. At very small spacings ($d/a < 1{\cdot}5$) the flow field cannot be computed accurately owing to the insufficient convergence of the spherical constant coefficients $B_n$ and $D_n$. In this case, as demonstrated by Davis *et al.* (1976), the number of ring vortices increases and a very complex wake structure is formed. The formation of the primary ring vortices and their coalescence into one vortex shown in figure 5 was examined by calculating the fluid velocity on the axis of symmetry $R = 0$ in the gap between the sphere and the disk. The lengths of the separated flow regions near the sphere ($l_s$) and near the disk ($l_d$) are shown in figure 6 as functions of sphere-to-disk spacing $d$. One

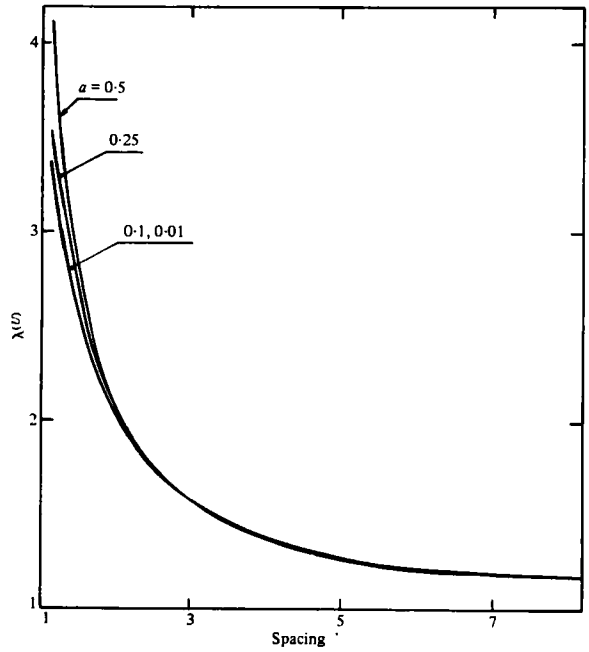


FIGURE 7. Rescaled hydrodynamic correction factor for uniform flow past a sphere–disk configuration for small values of $a$.

notes that the separated flow regions on the disk are both much larger and form at significantly larger separation distances than the sphere.

Although the flow field shown in figures 4 and 5 demonstrates clearly the separation of the flow from the boundaries, it does not offer an explanation for the increased drag on the sphere. Intuitively, this behaviour might result from the weak singularity in the pressure and the shear-stress fields at $R = 1$, which introduce high shear rates and pressure gradients in the vicinity of the disk edge that affect the force on the sphere when it is larger than the disk and in close proximity. In this context it should be noted that, although the drag on the sphere exceeds the value of the drag on an isolated sphere in a uniform stream, the total drag force on the sphere and the disk combined is smaller than the sum of the drag forces on an isolated sphere and an isolated disk in uniform flow.

Finally, it is important to examine the behaviour of the drag force on a rigidly held sphere in the limit when the disk radius becomes much larger than that of the sphere. For this purpose an alternative expression for the drag force can be written by introducing the undisturbed local fluid velocity as follows:

$$F = 6\pi a U \lambda^{(U)}, \tag{3.2}$$

where $U$ is the velocity on the disk axis and is given in Sampson (1891) for flow past a disk in the absence of the sphere by

$$\frac{U}{U_\infty} = \left[1 - \frac{2}{\pi}\left(\operatorname{arccot} d + \frac{d}{1+d^2}\right)\right]. \tag{3.3}$$

Comparing (3.2) and (2.20$b$) we can write

$$\lambda^{(U)} = \lambda^{(U_\infty)} \frac{U_\infty}{U}. \tag{3.4}$$

Results for $\lambda^{(U)}$ are plotted in figure 7. Clearly, for small values of $a$ the results converge into a single curve independent of that value.

## 4. Solutions for the drag force acting on the disk

The expression for the drag force acting on the disk in the presence of the sphere can be obtained by integrating the pressure over both the left and right surfaces. The normal and tangential shear-stress components on the surface of the disk have no contribution to the drag force. The normal component $\partial u_z/\partial z$, which can be expressed via the continuity equation in terms of the radial velocity component $(1/R)\,\partial R u_R/\partial R$, vanishes at $z = d$ and $R < 1$. The tangential component acts in the radial direction and, therefore, has no effect on the force in the $z$-direction. Hence

$$\begin{aligned} F_{\mathrm{d}} &= 2\pi \int_0^1 p^{\mathrm{I}}(R,d) - p^{\mathrm{II}}(R,d)\, R\, dR \\ &= 16U_\infty + 16 \sum_{n=2}^{\infty} \left\{ B_n \frac{S_n(d)}{n} + D_n \frac{2n-3}{n(n-1)} dS_{n-1}(d) \right. \\ &\qquad \left. - D_{n+1} \frac{n-2}{n^2-1} S_{n-1}(d) \right\} + \tfrac{1}{2} D_2 \operatorname{arccot} d, \end{aligned} \tag{4.1}$$

where $S_n(d)$ is given by

$$S_n(d) = (1+d^2)^{-\frac{1}{2}n} \sin(n \operatorname{arccot} d). \tag{4.2}$$

Clearly, when the sphere is far from the disk ($d \to \infty$), (4.1) reduces to

$$F_{\mathrm{d}} = 16U_\infty, \tag{4.3}$$

which is in agreement with the exact solution for uniform flow past a disk in the absence of the sphere (Sampson 1891).

The dimensionless drag force $F_{\mathrm{d}}$ was computed for both cases when the sphere is translating towards the disk and for the flow past the stationary sphere–disk configuration. The drag correction factor for these two flows is defined respectively by

$$\lambda_{\mathrm{d}}^{(V)} = F_{\mathrm{d}}^{(V)}/16V, \tag{4.4$a$}$$

$$\lambda_{\mathrm{d}}^{(U_\infty)} = F_{\mathrm{d}}^{(U_\infty)}/16U_\infty, \tag{4.4$b$}$$

where $U_\infty$ is the uniform stream velocity and $V$ is the sphere velocity.

Results for $\lambda_{\mathrm{d}}^{(V)}$ and $\lambda_{\mathrm{d}}^{(U_\infty)}$ are shown in figures 8 and 9 respectively. Inspection of figure 8 reveals that the drag on the disk increases monotonically with decreasing spacing when the sphere is moving towards the disk in quiescent fluid. When both the sphere and the disk are fixed in the uniform stream (figure 9), the drag on a disk smaller than the sphere ($a > 1$) decreases with decreasing gap width to its minimum value at contact. However, when $a < 1$, the value of the drag is smallest before contact and increases slightly with decreasing gap width. Additional computations have shown that the value of $a$ at which this transition takes place is about 0·86. A similar behaviour of the drag force has been shown for the motion of two unequal spheres

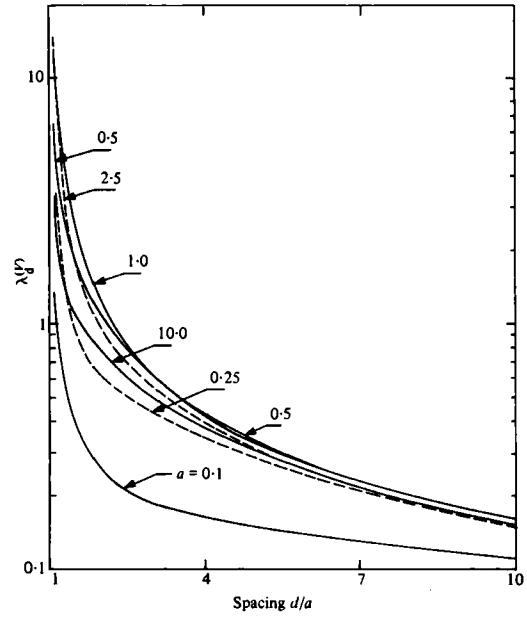


FIGURE 8. Drag on a disk due to an axisymmetric motion of a sphere. (The dashed curves are used for clarity.)

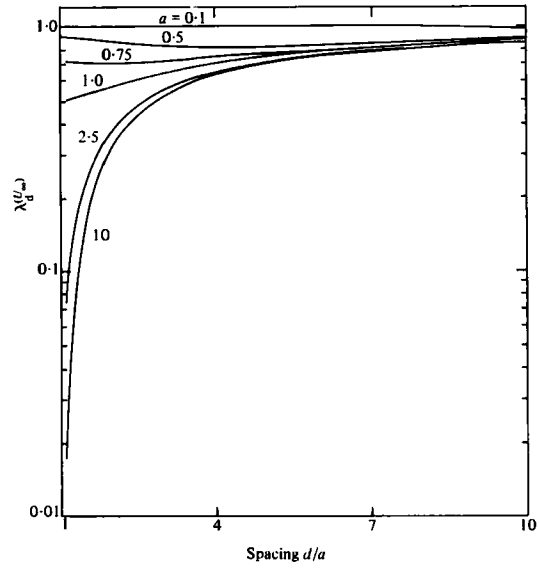


FIGURE 9. Drag on a disk in a uniform flow past a sphere–disk configuration.

along their line of centres (Cooley & O'Neill 1969). Furthermore, this phenomenon can be also seen in figure 3 for the drag acting on the sphere in the same flow conditions. In this case the transition occurs when the value of $a$ is about 1·08.

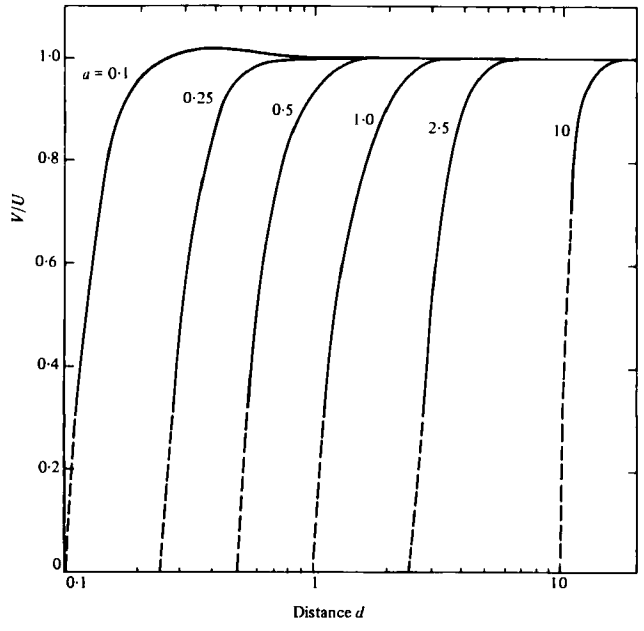


FIGURE 10. Velocity of a neutrally buoyant sphere carried by a uniform flow towards a disk. – – – –, extrapolated results.

## 5. The axisymmetric motion of a neutrally buoyant sphere carried by a uniform flow towards a stationary disk

In this section the motion of a neutrally buoyant sphere carried by the flow towards a stationary disk is considered by superposing the two solutions presented in § 3.

Using (2.22) and requiring zero net force on the sphere, one can obtain the expression for the sphere velocity $V$ in the form

$$\frac{V}{U_\infty} = -\frac{\lambda^{(U_\infty)}}{\lambda^{(V)}}. \tag{5.1}$$

Equation (5.1) can be written in an alternative form by using the expression for the centre-line undisturbed local fluid velocity (3.3). Hence, (5.1) becomes

$$\frac{V}{U} = -\frac{\lambda^{(U_\infty)}}{\lambda^{(V)}}\left[1-\frac{2}{\pi}\left(\operatorname{arccot} d+\frac{d}{1+d^2}\right)\right]^{-1}. \tag{5.2}$$

Equation (5.2) is plotted in figure 10 for various sphere sizes, indicating that the sphere velocity increases above the local fluid velocity before it decays to zero as the sphere approaches the disk. The dashed extensions in this figure are extrapolated results for $d/a < 1{\cdot}1$. Note that the actual distance $d$ is plotted rather than $d/a$ so that the curves should not overlap.

## 6. Application of the solution technique in future research

This paper presents a matching technique for treating complex flow geometries where the field is divided into simply bounded regions which are matched kinematically and dynamically along the interface between the regions. The paper also demonstrates

that the boundary-collocation technique can be used efficiently in axisymmetric flows containing discontinuous planar surfaces that cannot be defined by a natural co-ordinate system.

The boundary-collocation-series technique presented herein and its extension to unbounded (Ganatos, Pfeffer & Weinbaum 1978) and bounded (Ganatos, Pfeffer & Weinbaum 1980; Ganatos, Weinbaum & Pfeffer 1980) three-dimensional motion of spheres can be applied to a wide variety of unsolved strong-interaction problems such as the motion of a sphere into a two-dimensional slit, the three-dimensional motion of a sphere into a pore, the off-axis motion of a sphere in a circular cylinder or the tumbling of a spheroid near a planar boundary. A serious limitation of the solution technique is the long computation time required for the numerical evaluation of the inversion integrals representing the disturbances generated by the confining boundaries. Special care must therefore be taken in writing an efficient program in order to avoid repetitive calculations.

In the past decade two other solution techniques have been introduced for treating more varied boundary-value problems involving mixed or non-orthogonal co-ordinate systems: the finite-element method and an integral-equation approach. At the request of one of the referees we have briefly outlined the advantages and disadvantages of each approach compared with the boundary-collocation-series technique used in this and previous studies by the authors, to help the reader decide which is the most efficient technique for treating future problems. The application of finite-element methods to low-Reynolds-number flow problems has thus far been confined to two-dimensional or axially symmetric finite-domain problems. This is an approximate numerical method (approximating functions used in each element do not satisfy the governing differential equations exactly but in some optimal average sense) whose most important advantage is that it can treat irregular body shapes. An interesting application of the method, which demonstrates this versatility, is the paper by Skalak *et al.* (1972) on the axially symmetric motion of irregular-shaped rouleaux periodically distributed along the axis of a circular cylinder. The periodicity requirement is important since it reduces the domain to finite dimensions. At present the principal drawbacks of this method are that it is difficult to treat infinite boundaries or three-dimensional motions.

The integral-equation approach and the boundary-collocation technique employed herein differ fundamentally from the finite-element method in that each of the terms in the solution is an exact solution of the governing Stokes slow-flow equation. The principal difference between the integral-equation solution and the boundary technique is that in the former one introduces a continuous distribution of fundamental solutions (Green functions) at the surface of the body to be represented that already satisfies the no-slip boundary conditions at all other boundaries in the flow, whereas in the latter one represents the body by a uniformly truncated series of specially chosen internal singularities that are compatible with the natural orthogonal co-ordinate geometry of the body. In the integral-equation approach the essential mathematical problem is to find the Green function (commonly called Stokeslet) that satisfies the viscous-flow boundary conditions at all other boundaries. In the boundary-collocation technique the equivalent mathematical problem is to find the Fourier integral representation of the wall disturbances that satisfies the boundary conditions on the confining walls for each order internal singularity. The important advantages of the

boundary approach are that the singularities representing the body are relatively simple since they do not have to satisfy the no-slip boundary conditions on the confining walls (the distribution of wall singularities is required to do this) and they are a natural co-ordinate expansion or in some sense an optimal representation of the body geometry. Thus, for a finite body that conforms to some orthogonal co-ordinate geometry the boundary-collocation technique will be a substantially more efficient approach than a numerical integral-equation solution. This is easily illustrated by considering the flow geometry in the present paper or its complementary study, the axial motion of a sphere towards an orifice (Dagan *et al.* 1982*b*). To apply the integral-equation method, one would first have to determine the three-dimensional motion of a Stokeslet approaching a disk or orifice. This is a difficult mathematical problem for the general three-dimensional case. The only existing solution is for the axial motion towards an orifice (Davis, O'Neill & Brenner 1981). This fundamental solution would then be integrated in the azimuthal direction around the surface of the body to find the basic ring singularity that satisfies the no-slip conditions on the disk or orifice walls (for the equivalent problem of an axisymmetric body in unbounded flow see Youngren & Acrivos 1975).† Finally, a superposition integral would be written using the ring singularity just described as the kernel of an integral equation for the unknown surface singularity distribution.

There are, however, types of problems for which the integral-equation approach is either better suited or perhaps the only approach. This is in general true for the motion of slender bodies near boundaries. The motion of a Stokeslet near one wall (Blake 1971), between two parallel plane walls (Liron & Mochon 1976) or in a circular cylinder (Liron & Shahar 1978) serves as the Green function for these problems. For non-slender bodies that do not conform to orthogonal co-ordinate surfaces, the boundary collocation technique can still be used, but the convergence of the truncation series is difficult to predict. For example, point-centred or distributed spherical solutions can be used, and a good numerical approximation obtained for non-spherical bodies, but the solutions may not be uniformly convergent (for a discussion of the equivalent unbounded axisymmetric body problem see the appendix in Gluckman *et al.* 1972). Thus, for more varied axisymmetric three-dimensional objects the extension of the integral technique of Youngren & Acrivos (1975) to bounded-flow problems might be required. However, as a general rule for bodies that do conform to a natural co-ordinate geometry the boundary-collocation technique would be the preferred approach, since it provides a more efficient description of the disturbance produced by the body.

The authors wish to thank the National Science Foundation for supporting this research under grant ENG-78-22101 and The City University of New York Computer Center for the use of their facilities. The above work has been performed in partial fulfilment of the requirements for the Ph.D. degree of Z. Dagan from The School of Engineering of The City College of The City University of New York.

† The Green function derived in Gluckman *et al.* (1971) for an arbitrary axisymmetric body is based on an oblate spheroidal singularity of vanishing aspect ratio rather than a ring Stokeslet. This is really an internal singularity whose focal ring lies on the surface of the body. The integral equation obtained in Gluckman *et al.*, while equivalent to that in Youngren & Acrivos, has a different kernel.

## Appendix A

This appendix contains a listing of the functions in (2.9):

$$\beta'_n(R,z) = B'_n(R,z) - B'_n(R,2d-z) + 2(d-z)(n+1)B'_{n+1}(R,2d-z), \tag{A 1}$$

$$\delta'_n(R,z) = D'_n(R,z) - D'_n(R,2d-z) - (2/n)(n-1)(n-3)(d-z)B'_{n-1}(R,2d-z) + 2(2n-3)d(d-z)B'_n(R,2d-z), \tag{A 2}$$

$$\beta''_n(R,z) = B''_n(R,z) - B''_n(R,2d-z) - 2(d-z)(n+1)B''_{n+1}(R,2d-z), \tag{A 3}$$

$$\delta''_n(R,z) = D''_n(R,z) - D''_n(R,2d-z) + 2(n-2)(d-z)B''_{n-1}(R,2d-z) - 2(2n-3)d(d-z)B''_n(R,2d-z), \tag{A 4}$$

where

$$B'_n(R,z) = \frac{n+1}{(R^2+z^2)^{\frac{1}{2}n}}\frac{1}{R}I_n\left(\frac{z}{(R^2+z^2)^{\frac{1}{2}}}\right), \tag{A 5}$$

$$D'_n(R,z) = \frac{n+1}{(R^2+z^2)^{\frac{1}{2}(n-2)}}\frac{1}{R}I_{n+1}\left(\frac{2}{(R^2+z^2)^{\frac{1}{2}}}\right) - \frac{2}{(R^2+z^2)^{\frac{1}{2}(n-1)}}\frac{z}{R}I_n\left(\frac{z}{(R^2+z^2)^{\frac{1}{2}}}\right), \tag{A 6}$$

$$B''_n(R,z) = \frac{1}{(R^2+z^2)^{\frac{1}{2}(n+1)}}P_n\left(\frac{z}{(R^2+z^2)^{\frac{1}{2}}}\right), \tag{A 7}$$

$$D''_n(R,z) = \frac{1}{(R^2+z^2)^{\frac{1}{2}(n-1)}}I_n\left(\frac{z}{(R^2+z^2)^{\frac{1}{2}}}\right) + \frac{1}{(R^2+z^2)^{\frac{1}{2}(n-1)}}P_n\left(\frac{z}{(R^2+z^2)^{\frac{1}{2}}}\right), \tag{A 8}$$

$P_n$ are Legendre polynomials of order $n$, and $I_n$ are Gegenbauer functions of the first kind of order $n$ and degree $-\frac{1}{2}$.

## Appendix B

This appendix contains a listing of the $A_i(\omega)$ and $B_i(\omega)$ functions ($i = 1, 2$) contained in (2.3) and (2.5) in terms of the unknown velocity in the plane of the disk and the unknown spherical coefficients $B_n$ and $D_n$:

$$A_1(\omega)\,e^{\omega d} = (1+\omega d)\int_1^\infty f(\xi)J_0(\omega\xi)\,d\xi - \omega\int_1^\infty g(\xi)J_1(\omega\xi)\,d\xi - \sum_{n=2}^{\infty}\{B_n[B_n^{**}(\omega,d)(1+\omega d)+\omega\,dB_n^{*}(\omega,d)] + D_n[D_n^{**}(\omega,d)(1+\omega d)+\omega\,dD_n^{*}(\omega,d)]\} - U_\infty\left(\frac{1}{\omega}+d\right)J_1(\omega), \tag{B 1}$$

$$B_1(\omega)\,e^{\omega d} = \omega\left[\int_1^\infty g(\xi)J_1(\omega\xi)\,d\xi - \int_1^\infty f(\xi)J_0(\omega\xi)\,d\xi\right] + \omega\sum_{n=2}^{\infty}\{B_n[B_n^{*}(\omega,d)+B_n^{**}(\omega,d)]+D_n[D_n^{*}(\omega,d)+D_n^{**}(\omega,d)]\} + U_\infty J_1(\omega), \tag{B 2}$$

$$A_2(\omega)\,e^{-\omega d} = (1-\omega d)\int_1^\infty f(\xi)J_0(\omega\xi)\,d\xi - \omega d\int_1^\infty g(\xi)J_1(\omega\xi)\,d\xi - (1-\omega d)U_\infty\frac{J_1(\omega)}{\omega}, \tag{B 3}$$

$$B_2(\omega)\,e^{-\omega d} = \omega\left[\int_1^\infty f(\xi)J_0(\omega\xi)\,d\xi + \int_1^\infty g(\xi)J_1(\omega\xi)\,d\xi\right] - U_\infty J_1(\omega), \tag{B 4}$$

where

$$B_n^*(\omega,d)=\int_0^\infty B_n'(t,d)\,tJ_1(\omega t)\,dt=\frac{\omega^{n-1}}{n!}e^{-\omega d}, \tag{B 5}$$

$$D_n^*(\omega,d)=\int_0^\infty D_n'(t,d)\,tJ_1(\omega t)\,dt=\frac{\omega^{n-3}}{n!}[(2n-3)\,\omega d-n(n-2)]\,e^{-\omega d}, \tag{B 6}$$

$$B_n^{**}(\omega,d)=\int_0^\infty B_n''(t,d)\,tJ_0(\omega t)\,dt=\frac{\omega^{n-1}}{n!}e^{-\omega d}, \tag{B 7}$$

$$D_n^{**}(\omega,d)=\int_0^\infty D_n''(t,d)\,tJ_0(\omega t)\,dt=\frac{\omega^{n-3}}{n!}[(2n-3)\,\omega d-(n-1)\,(n-3)]\,e^{-\omega d}. \tag{B 8}$$

## Appendix C

This appendix contains a listing of the functions $F^*$ and $G^*$ appearing on the right-hand side of the integral equations (2.12):

$$F^*(R)=\frac{1}{2}\int_0^\infty\left\{\sum_{n=2}^\infty B_n[B_n^*(\omega,d)+B_n^{**}(\omega,d)]+D_n(D_n^*[\omega,d)+D_n^{**}(\omega,d)]\right\}\omega^2J_0(\omega R)\,d\omega$$
$$+\frac{1}{2}\sum_{n=2}^\infty D_n\frac{2n-3}{n}B_{n-1}''(R,d), \tag{C 1}$$

$$G^*(R)=-\frac{1}{2}\int_0^\infty\left\{\sum_{n=2}^\infty B_n[B_n^*(\omega,d)+B_n^{**}(\omega,d)]+D_n[D_n^*(\omega,d)\right.$$
$$\left.+D_n^{**}(\omega,d)]\right\}\omega^3J_0(\omega R)\,d\omega+\frac{1}{2}\sum_{n=2}^\infty D_n(2n-3)\,B_n''(R,d), \tag{C 2}$$

where $B_n^*$, $B_n^{**}$, $D_n^*$ and $D_n^{**}$ are given in appendix B.

## Appendix D

This appendix contains the definitions and evaluation of the functions in (2.17):

$$\mathscr{B}_n^*(R,z,t)=(n+1)\,C_{n+2}(t,d)\,[Q_1^{-1}(R,X,t)-xQ_1^0(R,x,t)]-xC_{n+1}(t,d)\,Q_1^{-1}(R,x,t), \tag{D 1}$$

$$\mathscr{D}_n^*(R,z,t)=[(2n-3)\,dC_{n+1}(t,d)-(n-2)\,C_n(t,d)]\,[Q_1^{-1}(R,x,t)-xQ_1^0(R,x,t)]$$
$$+\frac{x}{n}Q_1^1(R,x,t)\,[(n-3)\,C_{n-1}(t,d)-(2n-3)\,dC_n(t,d)], \tag{D 2}$$

$$\mathscr{B}_n^{**}(R,z,t)=Q_0^0(R,x,t)\,[C_{n+1}(t,d)+x(n+1)\,C_{n+2}(t,d)]+xQ_0^1(R,x,t)\,C_{n+1}(t,d), \tag{D 3}$$

$$\mathscr{D}_n^{**}(R,z,t)=[Q_0^0(R,x,t)+xQ_0^1(R,x,t)]\left[\frac{2n-3}{n}dC_n(t,d)-\frac{n-3}{n}C_{n-1}(t,d)\right]$$
$$+Q_0^0(R,x,t)\,x[(2n-3)\,dC_{n+1}(t,d)-(n-2)\,C_n(t,d)], \tag{D 4}$$

where

$$S_\nu^\mu(R,x)=\int_0^\infty\omega^\mu J_\nu(\omega R)\,e^{-\omega x}\sin\omega\,d\omega, \tag{D 5}$$

$$Q_\nu^\mu(R,x,t)=\int_0^\infty\omega^\mu J_\nu(\omega R)\,e^{-\omega x}\cos\omega t\,d\omega, \tag{D 6}$$

$$C_n(t,d)=\frac{\cos(n\arctan t/d)}{(t^2+d^2)^{\frac{1}{2}n}}. \tag{D 7}$$

The integrals defined by (D 5), (D 6) can be evaluated using the results in Erdélyi *et al.* (1954, vol. 1, p. 101; vol. 2, pp. 11, 19). Then

$$S_1^0(R,x) = \frac{x(1-h_1^2)}{Rh_1\sigma_1}, \tag{D 8a}$$

$$S_0^0(R,x) = h_1/\sigma_1, \tag{D 8b}$$

$$Q_1^{-1}(R,x,t) = \frac{h-x}{R}, \tag{D 9a}$$

$$Q_1^0(R,x,t) = \frac{1}{R}\left[1-x\frac{t^2+h^2}{h\sigma}\right], \tag{D 9b}$$

$$Q_0^0(R,x,t) = h/\sigma, \tag{D 9c}$$

$$Q_0^1(R,x,t) = \frac{x}{\sigma^2}\left[\frac{4h(t^2+h^2)}{\sigma} - \frac{t^2+3h^2}{h}\right], \tag{D 9d}$$

$$Q_1^1(R,x,t) = \frac{t^2+h^2}{Rh\sigma}\left[1+\frac{4x^2}{\sigma} - \frac{x^2(t^2+h^2)}{\sigma}\left(\frac{1}{h^2}+\frac{4}{\sigma}\right)\right], \tag{D 9e}$$

where $h$ and $h_1$ are the roots of the algebraic equations

$$b^4 - b^2(R^2+x^2-t^2) - x^2t^2 = 0, \tag{D 10a}$$

$$h_1^4 + h_2^2(R^2+x^2-1) - x^2 = 0, \tag{D 10b}$$

and $\sigma$ and $\sigma_1$ are defined by

$$\sigma = [(R^2+x^2-t^2)^2 + 4x^2t^2]^{\frac{1}{2}}, \tag{D 11a}$$

$$\sigma_1 = [(R^2+x^2-1)^2 + 4x^2]^{\frac{1}{2}}. \tag{D 11b}$$

The solution (2.17) satisfies the no-slip boundary conditions on the surface of the disk and the stress-tensor matching condition with region II for any value of the constant coefficients $B_n$ and $D_n$. The single integrals in the infinite series in (2.17) must be performed numerically. In this regard, it should be noted that the expressions for $Q_1^{-1}$ and $Q_1^0$ given by (D 9$a$, $b$) are prone to large round-off errors when $R$ is small and $h \sim x$. Therefore $Q_1^{-1}$ should be computed using the substitution

$$h-x = \frac{R^2h^2}{(h^2+t^2)(h+x)}, \tag{D 12}$$

which results directly from (D 10$a$). $Q_1^0$ can be obtained in an alternative form by differentiating $Q_1^{-1}$ with respect to $x$. Hence

$$Q_1^0(R,x,t) = \frac{R}{h+x}\left[\frac{h^2}{h^2+t^2}\left(\frac{2x}{\sigma}+\frac{1}{h+x}\right) + \frac{x}{\sigma}\left(\frac{h}{h+x}-\frac{2}{\sigma}\right)\right]. \tag{D 13}$$

## REFERENCES


Blake, J. R. 1971 *Proc. Camb. Phil. Soc.* **70**, 303.

Brenner, H. 1961 *Chem. Engng Sci.* **16**, 242.

Cooley, M. D. A. & O'Neill, M. E. 1969 *Proc. Camb. Phil. Soc.* **66**, 407.

Dagan, Z. 1980 Entrance effects in Stokes flow through a pore. Ph.D. dissertation, City University of New York.

DAGAN, Z., WEINBAUM, S. & PFEFFER, R. 1982*a* *J. Fluid Mech.* **115**, 505.

DAGAN, Z., WEINBAUM, S. & PFEFFER, R. 1982*b* *J. Fluid Mech.* **117**, 143.

DAVIS, A. M. J., O'NEILL, M. E., DORREPAAL, J. M. & RANGER, K. B. 1976 *J. Fluid Mech.* **77**, 625.

DAVIS, A. M. J., O'NEILL, M. E. & BRENNER, H. 1981 *J. Fluid Mech.* **103**, 183.

ERDÉLYI, A., MAGNUS, W., OBERHETTINGER, F. & TRICOMI, F. G. 1954 *Tables of Integral Transforms*, vols 1, 2. McGraw-Hill.

GANATOS, P., PFEFFER, R. & WEINBAUM, S. 1978 *J. Fluid Mech.* **84**, 79.

GANATOS, P., PFEFFER, R. & WEINBAUM, S. 1980 *J. Fluid Mech.* **99**, 755.

GANATOS, P., WEINBAUM, S. & PFEFFER, R. 1980 *J. Fluid Mech.* **99**, 739.

GLUCKMAN, M. J., PFEFFER, R. & WEINBAUM, S. 1971 *J. Fluid Mech.* **50**, 705.

GLUCKMAN, M. J., WEINBAUM, S. & PFEFFER, R. 1972 *J. Fluid Mech.* **69**, 677.

HAPPEL, J. & BRENNER, H. 1973 *Low Reynolds Number Hydrodynamics*, 2nd edn. Noordhoff.

LIAO, W. H. & KRUEGER, D. A. 1980 *J. Fluid Mech.* **96**, 223.

LIRON, N. & MOCHON, S. 1976 *J. Engng Math.* **10**, 287.

LIRON, N. & SHAHAR, R. 1978 *J. Fluid Mech.* **86**, 727.

SAMPSON, R. A. 1891 *Phil. Trans. R. Soc. Lond.* A **182**, 449.

STIMSON, M. & JEFFERY, O. B. 1926 *Proc. R. Soc. Lond.* A **111**, 110.

TRANTER, C. J. 1951 *Q. J. Math.* **2**, 60.

WACHOLDER, E. & SATHER, M. F. 1974 *J. Fluid Mech.* **65**, 417.

YOUNGREN, G. K. & ACRIVOS, A. 1975 *J. Fluid Mech.* **69**, 813.